Simple approach for including foundation–soil–foundation interaction in the static stiffnesses of multi–element shallow foundations

J.D.R. Bordón[1], J.J. Aznárez[1], O. Maeso[1], and S. Bhattacharya[2]

[1]Instituto Universitario SIANI, Universidad de Las Palmas de Gran Canaria, 35017 Las Palmas de Gran Canaria, Spain

[2]Department of Civil and Environmental Engineering, University of Surrey, GU2 7XH Guildford, United Kingdom

Post-print of the paper originally published in Géotechnique (Online: May 14, 2020)

DOI: https://doi.org/10.1680/jgeot.19.P.005

Abstract

In common engineering practice, foundation–soil–foundation interaction of shallow foundations is frequently ignored. This is presumably due to cost/benefit reasons since computationally demanding finite and/or boundary element models are required for that purpose, and its effects are usually assumed as negligible. In this sense, the present paper provides a simple and inexpensive way of incorporating foundation–soil–foundation interaction through a numerically explicit stiffness matrix formulation. The necessary ingredients for homogeneous and non-homogeneous (shear modulus power-law variation with depth) half-spaces are given. The proposed approach is then applied to offshore wind turbines multiple suction caisson foundations (tripod and tetrapod), where it is observed that foundation–soil–foundation interaction is significant. Its range of validity is also established, and valuable ready-to-use closed-form formulas for the correction factors of the stiffnesses of tripod and tetrapod groups are also derived. The methodology is applicable as long as the spacing between foundations is somewhat greater than foundation depth.

Keywords: elasticity footings/foundations offshore engineering soil/structure interaction stiffness

1 Introduction

The problem of determining the static and dynamic stiffnesses of foundations is a classical problem in elasticity. The knowledge of the soil reaction to excitations arriving to the foundation from the superstructure or the underlaying soil is key to the appropriate design of the superstructure.

Back in the old days, researchers resorted to analytical and semi-analytical methods applied to canonical problems (typically a circular footing) which usually lead directly to closed-form formulas or methodologies of great simplicity, practical utility and physical insight. References to classical works in this field can be found in [Poulos and Davis, 1974]. Nowadays, the use of the numerical methods such as the Finite Element Method (FEM) and the Boundary Element Method (BEM) allows the treatment of more general problems, some of which can be found in the works of [Wolf, 1985] and [Domínguez, 1993]. However, building such models requires some expertise and it is time consuming. For these reasons, some researchers have put efforts in obtaining closed-form formulas and charts for stiffnesses fitted from numerical results, providing a great resource for engineers. The work of [Gazetas, 1991] is a well-known reference of this approach.

Compared to problems of isolated foundations, the problem of the interaction between foundations, i.e. Foundation–Soil–Foundation Interaction (FSFI), has received less attention. One exception is the case of pile foundations, where pile–to–pile interaction in pile groups, particularly in the problem of foundation elastic settlement, has received much attention, see for example the works of [Randolph and Wroth, 1979] and [Poulos and Davis, 1980]. The dynamic interaction between shallow foundations has also received attention, from which the works of [Wong, 1975] and [Wong and Luco, 1986] must be highlighted.

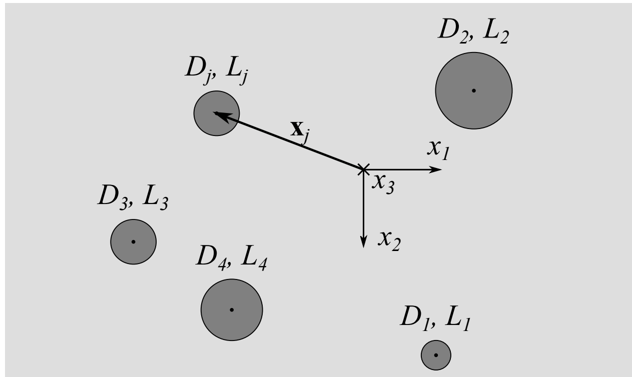

Figure 1: Arbitrary arrangement of shallow foundations

Inspired in the works of [Wong, 1975] and [Randolph and Wroth, 1979], the present paper generalizes some of their ideas, and it proposes a simple yet effective methodology for including a complete foundation–soil–foundation interaction in the stiffness matrices of foundation systems based on shallow foundations. The two main ingredients are the stiffness components for the isolated foundation and the Green's function for loads (point forces and moments) and observation (displacements and rotations) at the free-surface. Both can be found across the literature for different foundation geometries and soil profiles for static as well as dynamic analyses. In this paper, however, the simple case of the static analysis of cylindrical embedded rigid foundations in a homogeneous and non-homogeneous (shear modulus power-law variation with depth) half-space is considered. Under such hypotheses, a completely closed-form methodology which only requires some matrix operations can be formulated. The essential methodological contribution of this paper is the inclusion of the rotational degrees of freedom in the interaction. The main contribution of practical value is its application to polygonal arrangements of suction caisson foundations for Offshore Wind Turbines (OWT), which is a problem of great current interest.

2 Methodology

It is considered a linear elastic half-space ($x_3 \geq 0$), where a set of N axisymmetric rigid shallow foundations are arbitrarily arranged at surface points $\mathbf{x}_j = ({x_1}^{(j)}, {x_2}^{(j)}, 0)$ ($j = 1, 2, \ldots, N$) with diameter D_j and depth (embedment length) L_j, see Fig 1.

When each foundation j is subjected to a load vector $\mathbf{p}_j = ({f_1}^{(j)}; {f_2}^{(j)}; {f_3}^{(j)}; {m_1}^{(j)}; {m_2}^{(j)}; {m_3}^{(j)})$ (forces and moments at $\mathbf{x}_j$), the total displacement vector $\mathbf{a}_i = ({u_1}^{(i)}; {u_2}^{(i)}; {u_3}^{(i)}; {\theta_1}^{(i)}; {\theta_2}^{(i)}; {\theta_3}^{(i)})$ (displacements and rotations at $\mathbf{x}_i$) at each foundation i can be obtained by the principle of superposition as:

$$\mathbf{a}_i = \sum_{j=1}^{j=N} \mathbf{S}_{ij} \cdot \mathbf{p}_j, \; i = 1, \ldots, N \tag{1}$$

where each compliance matrix $\mathbf{S}_{ij}$ is a 6×6 matrix which relates the displacements of foundation i produced by the loads on foundation j. On one hand, the compliance matrix $\mathbf{S}_{ii}$ of self-interaction can be directly obtained from the inversion of the stiffness matrix $\mathbf{S}_{ii} = (\mathbf{K}_{ii})^{-1}$ for the isolated foundation i:

$$\mathbf{S}_{ii} = \begin{bmatrix} K_\mathrm{H} & 0 & 0 & 0 & K_\mathrm{SR} & 0 \\ & K_\mathrm{H} & 0 & -K_\mathrm{SR} & 0 & 0 \\ & & K_\mathrm{V} & 0 & 0 & 0 \\ & & & K_\mathrm{R} & 0 & 0 \\ & & & & K_\mathrm{R} & 0 \\ & & & & & K_\mathrm{T} \end{bmatrix}^{-1} \tag{2}$$

where K_H, K_V, K_R, K_SR and K_T are respectively the horizontal, vertical, rocking, coupled sway-rocking and torsional stiffnesses. Closed-form formulas for these are spread over the literature, see e.g. [Gazetas, 1991, Wolf, 1985], although they can also be calculated by means of numerical methods, see e.g. [Domínguez, 1993]. On the other hand, assuming that foundations i and j are sufficiently further away with regard to their dimensions, the compliance sub-matrix $\mathbf{S}_{ij}$ of mutual-interaction can be built from the complete displacements and rotations Green's function $\mathbf{G}(\mathbf{x}_{\text{load}}, \mathbf{x}_{\text{obs}})$ for point force and point moment loads as:

$$\mathbf{S}_{ij} = (\mathbf{G}(\mathbf{x}_j, \mathbf{x}_i))^T, i \neq j \tag{3}$$

where:

$$\mathbf{G}(\mathbf{x}_j, \mathbf{x}_i) = \begin{bmatrix} \begin{bmatrix} G_{f_l,u_k} \\ G_{m_l,u_k} \end{bmatrix} & \begin{bmatrix} G_{f_l,\theta_k} \\ G_{m_l,\theta_k} \end{bmatrix} \end{bmatrix} \tag{4}$$

is a 6×6 matrix composed of four 3×3 sub-matrices. In Eq. (4) subscripts denote the displacement u_k or rotation θ_k response due to a point force f_k or moment m_k $(k = 1, 2, 3)$.

Eq. (1) can also be written in a matrix form as:

$$\mathbf{a} = \mathbf{S} \cdot \mathbf{p} \tag{5}$$

where $\mathbf{S}$ is the $6N \times 6N$ complete system compliance matrix, $\mathbf{a} = (\mathbf{a}_1; \ldots; \mathbf{a}_i; \ldots; \mathbf{a}_N)$ is the $6N$ complete system displacement vector and $\mathbf{p} = (\mathbf{p}_1; \ldots; \mathbf{p}_i; \ldots; \mathbf{p}_N)$ is the $6N$ complete system load vector. Given that Green's function satisfies the reciprocity principle, then $\mathbf{S}_{ij} = \mathbf{S}_{ji}^T$, which together to the fact that $\mathbf{S}_{ii}$ is symmetric, proves that the complete system compliance matrix $\mathbf{S}$ is symmetric as expected. It should be recalled that $\mathbf{x}_j = ({x_1}^{(j)}, {x_2}^{(j)}, 0)$ and $\mathbf{x}_i = ({x_1}^{(i)}, {x_2}^{(i)}, 0)$, i.e. Green's function is evaluated for surface loads and responses, which is an appropriate simplifying assumption for shallow foundations or deep foundations sufficiently spaced apart, as it will be demonstrated later. Once the compliance matrix $\mathbf{S}$ is built, the complete foundation system stiffness matrix can directly be obtained by inversion:

$$\mathbf{p} = \mathbf{S}^{-1} \cdot \mathbf{a} = \mathbf{K} \cdot \mathbf{a} \tag{6}$$

This stiffness matrix can be easily plugged into a superstructure finite element model in order to take into account soil-structure interaction including foundation–soil–foundation effects.

Depending on the superstructure topology and dimensions, soil properties and the type of analysis to be performed, the supporting foundation system can be considered as rigidly connected. In that case, the overall soil-structure interaction can be reduced to a given master node. Consider that the master node is located at $\mathbf{x}_0$, and it has a displacement vector $\mathbf{a}_0 = ({u_1}^{(0)}; {u_2}^{(0)}; {u_3}^{(0)}; {\theta_1}^{(0)}; {\theta_2}^{(0)}; {\theta_3}^{(0)})$ and load vector $\mathbf{p}_0 = ({f_1}^{(0)}; {f_2}^{(0)}; {f_3}^{(0)}; {m_1}^{(0)}; {m_2}^{(0)}; {m_3}^{(0)})$. The kinematic master-slave relationship of a rigid link between the master node 0 and a given foundation node j is (see e.g. [Cook et al., 1989]):

$$\mathbf{a}_j = \mathbf{T}_j \cdot \mathbf{a}_0 = \begin{bmatrix} \mathbf{I}_{3\times 3} & \mathbf{D}_j \\ \mathbf{0}_{3\times 3} & \mathbf{I}_{3\times 3} \end{bmatrix} \cdot \mathbf{a}_0 \tag{7}$$

where $\mathbf{I}_{3\times 3}$ is a 3×3 identity matrix, $\mathbf{0}_{3\times 3}$ is a 3×3 zero matrix, and:

$$\mathbf{D}_j = \begin{bmatrix} 0 & {d_3}^{(j)} & -{d_2}^{(j)} \\ -{d_3}^{(j)} & 0 & {d_1}^{(j)} \\ {d_2}^{(j)} & -{d_1}^{(j)} & 0 \end{bmatrix} \tag{8}$$

where ${d_k}^{(j)} = {x_k}^{(j)} - {x_k}^{(0)}$. Hence, the complete system displacement vector can be written as:

$$\mathbf{a} = \begin{Bmatrix} \mathbf{a}_1 \\ \vdots \\ \mathbf{a}_j \\ \vdots \\ \mathbf{a}_N \end{Bmatrix} = \begin{bmatrix} \mathbf{T}_1 \\ \vdots \\ \mathbf{T}_j \\ \vdots \\ \mathbf{T}_N \end{bmatrix} \cdot \mathbf{a}_0 = \mathbf{T} \cdot \mathbf{a}_0 \tag{9}$$

The reduction of the load vector at foundation slave node j to the master node is simply:

$$\mathbf{p}_0^{(j)} = \mathbf{T}_j^T \cdot \mathbf{p}_j \tag{10}$$

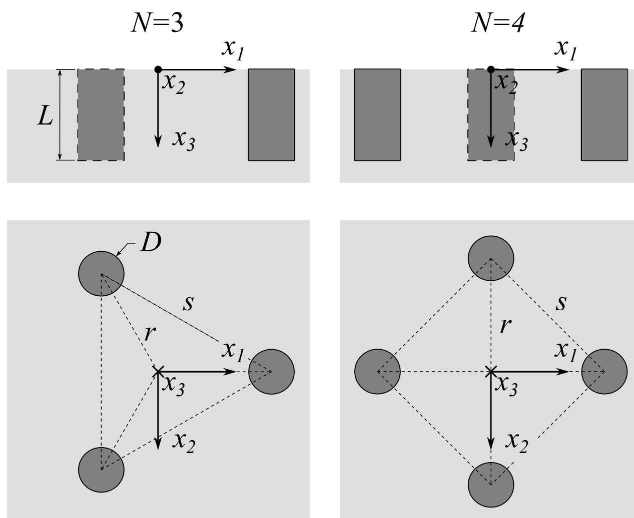

Figure 2: Tripod and tetrapod arrangements of suction caissons

which added together give the resultant load vector at the master node:

$$\mathbf{p}_0 = \sum_{j=1}^{j=N} \mathbf{p}_0^{(j)} = \mathbf{T}^T \cdot \mathbf{p} \tag{11}$$

Thus the stiffness matrix reduced to the master node can be obtained from:

$$\mathbf{K}_0 = \mathbf{T}^T \cdot \mathbf{K} \cdot \mathbf{T} \tag{12}$$

3 Application to OWT foundations

In this section, the above methodology is applied to a problem of current interest in the field of offshore wind turbines. This is the case of foundation systems supporting a jacket based on a polygonal arrangement of suction caisson foundations (also known as buckets or suction piles), which typically comprises three (tripod) or four (tetrapod) foundation elements.

According to [Houlsby and Byrne, 2005a, Houlsby and Byrne, 2005b], suction caissons can achieve length (depth) L to diameter D ratios up to $L/D \leq 1$ for sand soils, $L/D \leq 3$ for stiff clay soils and $L/D \leq 6$ for soft normally consolidated clay soils. The lid of suction caissons is always stiffened so that it can be considered as rigid. On the other hand, the skirt is flexible as it typically has thickness t to diameter D ratios around $t/D \sim 0.005$, although it may have stiffeners.

Regarding foundation static stiffnesses, suction caissons behave between rigid circular footings (for very flexible skirts) and a rigid cylindrical foundations (for very stiff skirts), see [Doherty and Deeks, 2003, Doherty et al., 2005]. [Doherty et al., 2005] obtained the stiffnesses of rigid and flexible suction caissons for a few Poisson's ratios ($\nu = \{0.2, 0.499\}$) and slendernesses ($L/D = \{0, 0.25, 0.5, 1.0, 2.0\}$), which come in the form of formulas and tables. More recently, [Efthymiou and Gazetas, 2018] obtained closed-form formulas for a flexible suction caisson with a fixed thickness, but their results are again limited up to $L/D = 2$. In the present paper, rigid cylindrical foundations with $0 \leq L/D \leq 6$ embedded in a homogeneous half-space are assumed, and a new set of modified Gazetas-type formulas is proposed, see Appendix A. In the case of rigid or flexible suction caissons in non-homogeneous half-spaces whose shear modulus follows a power-law with the depth ($\mu = \mu_0 \cdot z^\alpha$, $0 \leq \alpha \leq 1$), the stiffnesses presented by [Doherty et al., 2005] can be used.

Concerning the foundation system arrangement, it is considered that suction caissons are placed at the vertices of a regular N-sided polygon with radius r and side length (spacing) s ($s = 2r\sin(\pi/N)$). Fig. 2 shows a layout of the typical tripod ($N = 3$) and tetrapod ($N = 4$) cases. The origin of coordinates is located at the polygon center, and each foundation j is located at coordinates ${x_1}^{(j)} = r\cos(2\pi(j-1)/N)$ and ${x_2}^{(j)} = r\sin(2\pi(j-1)/N)$. For some analyses of OWT systems it is reasonable to assume a perfectly rigid connection between foundations, see e.g. [Jalbi and Bhattacharya, 2018]. In that case, it is possible to write an stiffness matrix reduced to a master node at the polygon center ($\mathbf{x}_0 = \mathbf{0}$).

The soil is considered whether as a homogeneous half-space with shear modulus μ and Poisson's ratio ν or a non-homogeneous half-space whose shear modulus following a power-law with the depth (as described before). In both cases, closed-form expressions for the Green's function $\mathbf{G}$ are available. They can be found in the Appendix B and C.

In order to measure the magnitude of foundation–soil–foundation interaction, it is first necessary to establish the reference case with no interaction. The construction of the complete stiffness matrix $\mathbf{K}$ is straightforward since from the very beginning it is possible to assume that $\mathbf{S}_{ij} = \mathbf{0}$ for $i \neq j$. The stiffness matrix reduced to the polygon center is easily obtained from Eq. (12), and it can be written as:

$$\mathbf{K}_0^{\text{no-int}} = N\mathbf{K}_{ii} + \frac{N}{2} r^2 \begin{bmatrix} 0 & 0 & 0 & 0 & 0 & 0 \\ & 0 & 0 & 0 & 0 & 0 \\ & & 0 & 0 & 0 & 0 \\ & & & K_\text{V} & 0 & 0 \\ & & & & K_\text{V} & 0 \\ & & & & & 2K_\text{H} \end{bmatrix} \tag{13}$$

which shows that the resulting foundation system behaves as an axisymmetric one.

Once foundation–soil–foundation interaction is considered, the resulting complete stiffness matrix $\mathbf{K}$ has to be obtained from the inversion of the complete compliance matrix $\mathbf{S}$ populated with the Green's function. $\mathbf{K}$ can be then introduced into a finite element model, which thus presents mutual foundation–soil–foundation interaction. In the case a rigid connection between foundations can be considered, the reduction of the complete stiffness matrix to the polygon center via Eq. (12) leads to the following reduced stiffness matrix $\mathbf{K}_0^{\text{int}}$:

$$\mathbf{K}_0^{\text{int}} = \begin{bmatrix} K_\text{H}^\text{int} & 0 & 0 & 0 & K_\text{SR}^\text{int} & 0 \\ & K_\text{H}^\text{int} & 0 & -K_\text{SR}^\text{int} & 0 & 0 \\ & & K_\text{V}^\text{int} & 0 & 0 & 0 \\ & & & K_\text{R}^\text{int} & 0 & 0 \\ & & & & K_\text{R}^\text{int} & 0 \\ & & & & & K_\text{T}^\text{int} \end{bmatrix} \tag{14}$$

which also represents an axisymmetric foundation. Unlike the case of no interaction, an amenable explicit expression for the five different components of the reduced stiffness matrix is not possible since $\mathbf{K}$ is a highly populated $6N \times 6N$ matrix. Therefore, it is generally preferable to obtain $\mathbf{K}_0^{\text{int}}$ numerically, which only requires a few matrix operations. In order to measure the magnitude of the foundation–soil–foundation interaction within the whole foundation system, the following group effect stiffness correction factors can be defined:

$$\gamma_\square = \frac{K_\square^\text{int}}{K_\square^\text{no-int}} \tag{15}$$

where $\square = \text{H}, \text{V}, \text{R}, \text{SR}, \text{T}$ denotes any of the stiffness components. They relate stiffnesses including interaction and stiffnesses not including it, and thus values of $\gamma_\square$ far from the unity indicate a strong foundation–soil–foundation interaction for the corresponding stiffness component, while values $\gamma_\square \sim 1$ indicate a small foundation–soil–foundation interaction. These factors are interesting not only because they measure the intensity of the foundation–soil–foundation interaction, but because they can be approximated by closed-form formulas. Approximate group effect stiffness correction factors $\gamma_\square$ have been presented in an earlier work [Bordón et al., 2019]. They were obtained via curve fitting of numerical results, and they consider tripod, tetrapod, pentapod and hexapod arrangements of rigid buckets up to $L/D \leq 1$ in homogeneous soils. In the present paper, the proposed methodology allows to cheaply obtain numerically or via closed-form formulas these factors for a much wider range of cases (deeper rigid or flexible caissons, homogeneous or non-homogeneous soils). For the sake of conciseness, only rigid skirts are considered since this is the most unfavorable situation for the proposed methodology.

The previously defined correction factors allow a partial introduction of foundation–soil–foundation interaction effects, which is only valid when the global response of the rigidly connected foundation system is required. The correction factors can be then easily used in standard finite element software by rigidly connecting all foundations to the master node. Then, an axisymmetric foundation is connected to the master node where the stiffness matrix $\mathbf{K}_0^{\text{int}}$ is populated with the following stiffness components:

$$K_{\text{V}}^{\text{int}} = \gamma_{\text{V}} N K_{\text{V}} \tag{16a}$$

$$K_{\text{H}}^{\text{int}} = \gamma_{\text{H}} N K_{\text{H}} \tag{16b}$$

$$K_{\text{R}}^{\text{int}} = \gamma_{\text{R}} N \left(K_{\text{R}} + \frac{s^2}{8\sin^2(\pi/N)} K_{\text{V}} \right) \tag{16c}$$

$$K_{\text{SR}}^{\text{int}} = \gamma_{\text{SR}} N K_{\text{SR}} \tag{16d}$$

$$K_{\text{T}}^{\text{int}} = \gamma_{\text{T}} N \left(K_{\text{T}} + \frac{s^2}{4\sin^2(\pi/N)} K_{\text{H}} \right) \tag{16e}$$

3.1 Homogeneous soil

In this section, the group effect stiffness correction factors are studied for the homogeneous soil, and the effects of the spacing s/D, number of foundations N (tripod or tetrapod), Poisson's ratio ν and slenderness L/D are analyzed. The present approach is also compared to rigorous numerical solutions and its validity range can be thus established.

Figs. 3 and 4 show how the group effect stiffness correction factors vary with the spacing s/D for $\nu = 0.2$ (typical for sand) and $\nu = 0.499$ (typical for clay and saturated soils), and tripod ($N = 3$) and ($N = 4$) tetrapod cases. It is also shown three different slenderness cases: $L/D = 0$ (surface foundation or suction caisson with a very flexible skirt), $L/D = 1$ (embedded foundation or typical suction caisson with rigid skirt in sand soils) and $L/D = 4$ (moderately deep foundation or typical suction caisson with rigid skirt in clay soils). Solid lines correspond to results obtained from a Boundary Element model (BE) [Bordón et al., 2017, Bordón et al., 2019], while dashed lines correspond to results of the proposed Simple Approach (SA). The following discussion is based on the results shown in these figures.

A very good agreement between results from both methodologies (BE and SA) is observed for $L/D = 0$, which, surprisingly, it is maintained even for very small spacings. For $L/D = 1$ there is still a very good agreement, but some peaks and an erratic behavior is obtained by the Simple Approach when $s/D \leq 2$ (only shown in Fig. 3 for $N = 3$ for the sake of clarity). Even for a moderately deep foundation with $L/D = 4$, there is a fairly good agreement for $s/D \geq 5$, whereas the erratic behavior appears for smaller spacings. This issue is however physically reasonable since foundations are embedded but the interaction between them is assumed to be at the surface. This inconsistency becomes apparent in the stiffness matrix after inverting the compliance matrix, and it will be further explained analytically later. The torsional mode is the worst mode reproduced by the Simple Approach, especially as L/D increases. Overall, the proposed simple approach works very well in practice, although its range of validity is limited by the main hypothesis of the interaction at the free-surface, which guarantees a good predictability only when the separation between foundations is somewhat greater than the foundation depth. From the present results, the range of validity can be established as $s/D > L/D + 1$.

Regarding the behavior of the vertical and horizontal stiffness correction factors, their most noticeable aspect is the fact that they are always smaller than one, i.e. foundation–soil–foundation interaction produces a stiffness reduction of the resulting group stiffness. This is a well-known phenomenon related to the fact that the translation of one foundation produces a translation in the same direction to the neighboring foundations, i.e. there is a helping effect between foundations which reduces the resulting stiffness. Ubiquitous Boussinesq's and Cerruti's solutions mainly govern such phenomena. The vertical and horizontal stiffness correction factors start from values smaller than one (around 0.5) at $s/D = 0$, and they tend to unity as the spacing increases. Naturally, they decrease as the slenderness increases, indicating that the increase of the foundation slenderness intensifies the influence of the foundation–soil–foundation interaction for any given s/D. Likewise, the correction is somewhat greater for the tetrapod than for the tripod. On the other hand, it is observed that Poisson's ratio has a small influence on correction factors. Overall, it is seen that the correction factors indicate a substantial stiffness reduction greater than 20% for spacings $s/D < 3$ when $L/D = 0$, $s/D < 4$ when $L/D = 1$, and $s/D < 8$ when $L/D = 4$.

The rocking stiffness correction factor exhibits a more complex behavior. For surface foundation ($L/D = 0$), it is greater than unity with a maximum of $\gamma_{\text{R}} \sim 1.1$ at approximately $s/D = 1.5$. It thus indicates a rocking stiffness increase due to foundation–soil–foundation interaction, which is only relevant for very small spacings. As the slenderness increases, the mentioned maximum moves to larger spacings and decreases until it almost disappears. Rocking stiffness correction factor has then a region below some spacing where it is smaller than unity. This approximately occurs when

$s/D < 3$ for $L/D = 1$, and when $s/D < 10$ for $L/D = 4$. A physical explanation for this intricate behavior can be given from the several helping and non-helping effects between foundations under the rocking mode. Helping effects tend to reduce the resulting stiffness (like in the vertical and horizontal case), and vice versa for non-helping effects. In [Bordón et al., 2019], a qualitative description of these effects are given. In the present paper, all these effects are quantified by some of the components of the complete 6×6 Green's function matrix (see Appendix B). For example, for $L/D = 0$ the rotation of a given foundation about the x_1-axis produces rotations in the opposite direction (non-helping effect) to foundations in front of ($x_1 = 0, x_2 > 0$) and behind ($x_1 = 0, x_2 < 0$), while it produces rotations in the same direction (helping effect) to foundations on both sides ($x_2 = 0$). This is described by G_{m_1,θ_1} (or G_{m_2,θ_2} if the rotation is about the x_2-axis).

The coupled sway-rocking stiffness correction factor presents a peculiarity, for surface foundations ($L/D = 0$) it does not tend to unity as the spacing increases. This effect is however negligible since this stiffness component can be generally neglected due to its small value when compared to horizontal and rocking stiffnesses. As the slenderness increases, the correction factor behaves similarly to the horizontal stiffness correction factor.

Regarding the torsional stiffness correction factor, it is observed curves similar to that of the rocking stiffness correction factor for $L/D = 0$. In this case, however, the correction is smaller and less sensitive to the slenderness. The correction reaches up to 20% increase or decrease depending on the case.

Given the relative simplicity of the formulation, it is possible to obtain analytical formulae of the stiffness correction factors with the help of a computer algebra system. Unfortunately, the obtained expressions are so complex that it is more appropriate to perform the numerical procedure instead. Nonetheless, if additional simplifications are made over the Green's function in each case, then more amenable and ready-to-use closed-form expressions can be obtained. In the following, such closed-form expressions are presented:

Vertical stiffness If only G_{f_3,u_3} is kept in the Green's function, the resulting group effect vertical stiffness correction factor has the following simple form:

$$\gamma_\mathrm{V} = \frac{1}{1 + \dfrac{q k_\mathrm{V}}{\tilde{s}}} \tag{17}$$

where $k_\mathrm{V} = K_\mathrm{V}/(\pi \mu D)$ is the dimensionless vertical stiffness (isolated foundation), $\tilde{s} = s/D$ is the dimensionless spacing, and coefficient q is:

$$N = 3: \; q = (1-\nu) \tag{18a}$$
$$N = 4: \; q = (1-\nu)(1+\sqrt{2}/4) \tag{18b}$$

Eq. (17) has been arranged so that it is easily interpretable and the relevant factors become dimensionless: coefficient q (which depends only on N and ν), dimensionless vertical stiffness k_V (which depends only on L/D and ν) and the reciprocal of the dimensionless spacing $1/\tilde{s}$. It is a monotonous function of $\tilde{s}$ which makes $\gamma_\mathrm{V} \to 0$ as $s/D \to 0$, and $\gamma_\mathrm{V} \to 1$ as $s/D \to \infty$. Figs. 3 and 4 show Eq. (17) using dash-dot lines, where it can be observed a good agreement when $s/D > L/D + 1$.

Horizontal stiffness If only G_{f_1,u_1} (or G_{f_2,u_2}) is kept in the Green's function, the resulting group effect horizontal stiffness correction factor can be written as:

$$\gamma_\mathrm{H} = \frac{1 + \dfrac{p_1 k_\mathrm{H}}{\tilde{s}}}{1 + \dfrac{q_1 k_\mathrm{H}}{\tilde{s}} + \dfrac{q_2 k_\mathrm{H}^2}{\tilde{s}^2}} \tag{19}$$

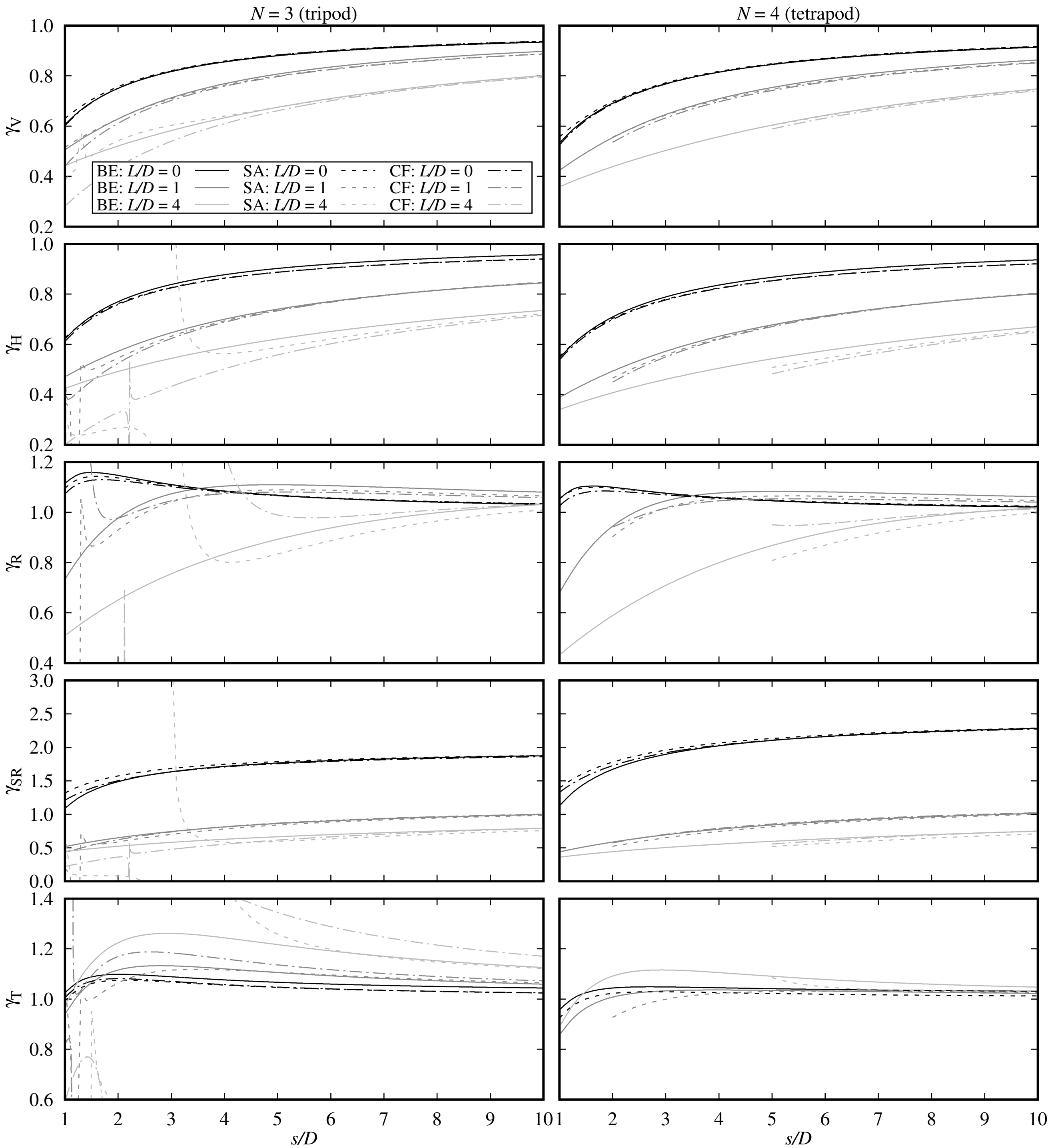

Figure 3: Stiffness correction factors for tripod and tetrapod arrangements of rigid suction caisson foundations ($\nu = 0.2$). BE: Boundary Element numerical solution (solid lines); SA: Simple Approach numerical solution (dashed lines) from Eqs. (15-16); CF: Closed-form Formulas (dash-dot lines) from Eqs. (17-27)

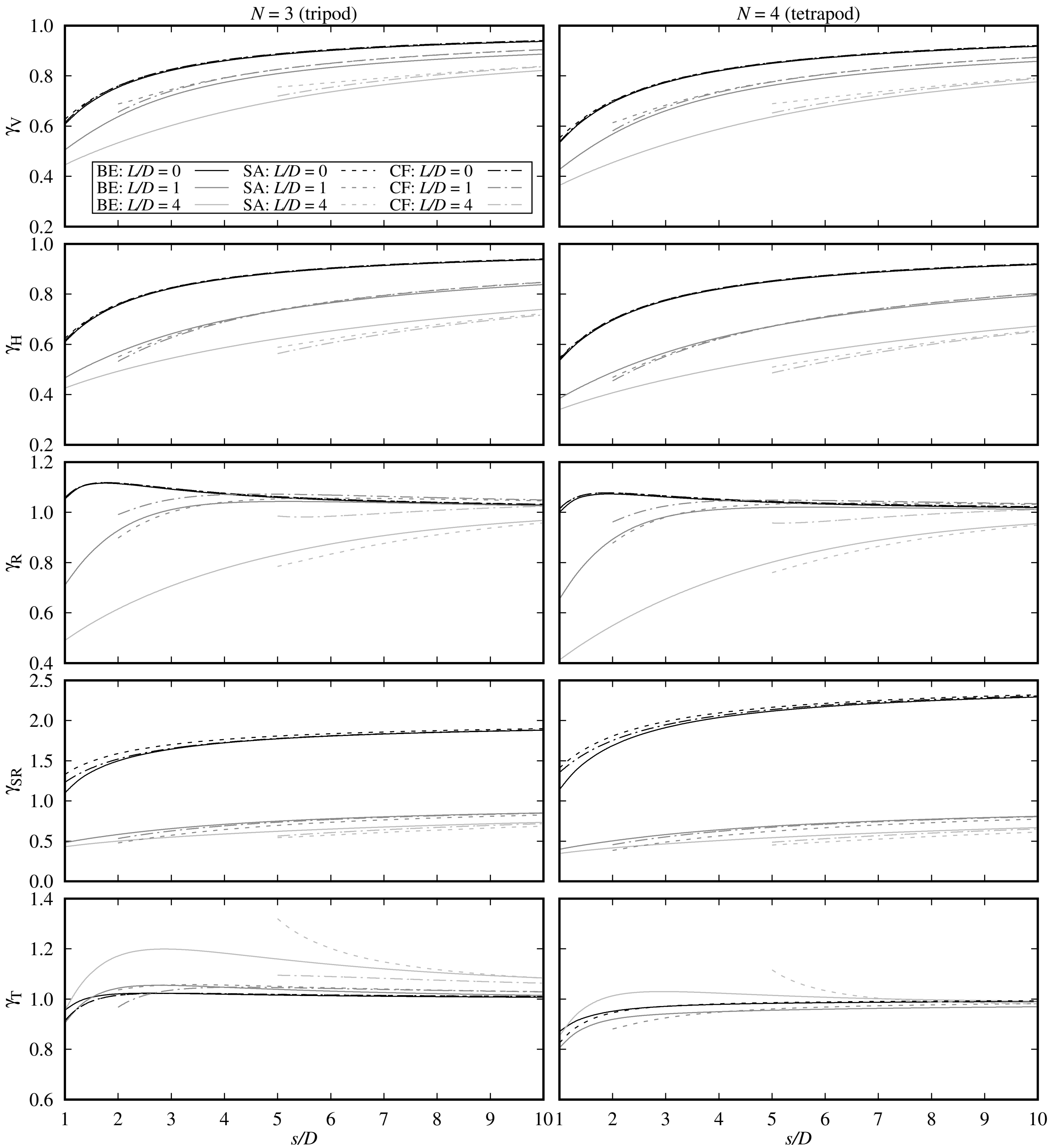

Figure 4: Stiffness correction factors for tripod and tetrapod arrangements of rigid suction caisson foundations ($\nu = 0.499$). BE: Boundary Element numerical solution (solid lines); SA: Simple Approach numerical solution (dashed lines) from Eqs. (15-16); CF: Closed-form Formulas (dash-dot lines) from Eqs. (17-27)

where $k_\mathrm{H} = K_\mathrm{H}/(\pi\mu D)$ is the dimensionless horizontal stiffness (isolated foundation), and p and q coefficients are:

$$N=3: \; p_1 = -1/2 \tag{20a}$$
$$q_1 = (1-\nu)/2 \tag{20b}$$
$$q_2 = -(4-\nu)^2/32 \tag{20c}$$
$$N=4: \; p_1 = -(2-\nu)(4-\sqrt{2})/8 \tag{20d}$$
$$q_1 = \sqrt{2}(2-\nu)/4 \tag{20e}$$
$$q_2 = -[7-\nu(7-2\nu)]/8 \tag{20f}$$

In this case, the rational function may present poles within the range of interest ($s/D \geq 1$), whose location depends on N, ν and k_H. As it was previously mentioned, the origin of this issue in the present approach is presumably due to the simplifying inconsistency of building self-interaction ($\mathbf{S}_{ii}$) for embedded foundations while mutual-interaction ($\mathbf{S}_{ij}$, $i \neq j$) is built for surface foundations. Figs. 3 and 4 show Eq. (19) using dash-dot lines, where it can be observed a very good agreement in the established validity range. The range where the erratic behavior is present is narrower than using the numerical procedure, although the discrepancy with respect boundary element results is somewhat greater.

Rotational stiffness By keeping G_{f_3,u_3}, G_{f_3,θ_1}, G_{m_1,u_3} and G_{m_1,θ_1} (or G_{f_3,u_3}, G_{f_3,θ_2}, G_{m_2,u_3} and G_{m_2,θ_2}) in the Green's function, it is possible to obtain the following group effect rotational stiffness correction factor:

$$\gamma_\mathrm{R} = \frac{1 + \dfrac{p_2 k_\mathrm{R}/k_\mathrm{V}}{\tilde{s}^2} + \dfrac{p_3 k_\mathrm{R}}{\tilde{s}^3} + \dfrac{p_5 k_\mathrm{R}^2/k_\mathrm{V}}{\tilde{s}^5} + \dfrac{p_6 k_\mathrm{R}^2}{\tilde{s}^6}}{\left(1 + \dfrac{p_2 k_\mathrm{R}/k_\mathrm{V}}{\tilde{s}^2}\right)\left(1 + \dfrac{q_1 k_\mathrm{V}}{\tilde{s}} + \dfrac{q_3 k_\mathrm{R}}{\tilde{s}^3} + \dfrac{q_4 k_\mathrm{R} k_\mathrm{V}}{\tilde{s}^4} + \dfrac{q_6 k_\mathrm{R}^2}{\tilde{s}^6} + \dfrac{q_7 k_\mathrm{R}^2 k_\mathrm{V}}{\tilde{s}^7}\right)} \tag{21}$$

where $k_\mathrm{R} = K_\mathrm{R}/(\pi\mu D^3)$ is the dimensionless rocking stiffness (isolated foundation), and p and q coefficients are:

$$N=3: \; p_2 = 6 \tag{22a}$$
$$p_3 = -7(1-\nu) \tag{22b}$$
$$p_5 = -3(1-\nu) \tag{22c}$$
$$p_6 = 95(1-\nu)^2/32 \tag{22d}$$
$$q_1 = -(1-\nu)/2 \tag{22e}$$
$$q_3 = -(1-\nu) \tag{22f}$$
$$q_4 = (1-\nu)^2/8 \tag{22g}$$
$$q_6 = -(1-\nu)^2/32 \tag{22h}$$
$$q_7 = 13(1-\nu)^3/64 \tag{22i}$$
$$N=4: \; p_2 = 4 \tag{22j}$$
$$p_3 = -(2+13\sqrt{2}/8)(1-\nu) \tag{22k}$$
$$p_5 = (2-\sqrt{2}/4)(1-\nu) \tag{22l}$$
$$p_6 = (4\sqrt{2}-39)(1-\nu)^2/16 \tag{22m}$$
$$q_1 = -\sqrt{2}(1-\nu)/4 \tag{22n}$$
$$q_3 = -\sqrt{2}(1-\nu)/8 \tag{22o}$$
$$q_4 = -(1-\nu)^2/2 \tag{22p}$$
$$q_6 = -5(1-\nu)^2/16 \tag{22q}$$
$$q_7 = 9\sqrt{2}(1-\nu)^3/128 \tag{22r}$$

Eq. (21) is considerably more complex than the previous estimations for vertical and horizontal correction factors. As in the horizontal case, the rational function also presents poles which contaminates the estimation for small s/D. Figs. 3 and 4 show Eq. (21) using dash-dot lines, where it can be observed that it is less accurate than results from the numerical procedure, especially as L/D increases. Nonetheless, it is a reasonable good estimator for $s/D > L/D + 1$.

Coupled sway-rocking stiffness By keeping all terms related to the lateral behavior in one plane, say plane $x_2 - x_3$: G_{f_2,u_2}, G_{f_2,u_3}, G_{f_2,θ_1}, G_{f_3,u_2}, G_{f_3,u_3}, G_{f_3,θ_1}, G_{m_1,u_2}, G_{m_1,u_3}, G_{m_1,θ_1}; it is possible to obtain closed-form expressions for γ_{SR} which match results from the SA numerical procedure. However, they are very lengthy, and it has not been possible to reduce them to an amenable form while maintaining a reasonable approximation. Unlike other stiffness components, the correction factor for the coupled sway-rocking stiffness does not tend to unity as the spacing increases (see Figs. 3 and 4). It has been possible to obtain the limiting values as:

$$N = 3: \lim_{s\to\infty} \gamma_{\mathrm{SR}} = 1 + \frac{(1-2\nu)}{8\pi}\frac{K_{\mathrm{H}}K_{\mathrm{V}}}{\mu K_{\mathrm{SR}}} \tag{23}$$

$$N = 4: \lim_{s\to\infty} \gamma_{\mathrm{SR}} = 1 + \frac{3(1-2\nu)}{16\pi}\frac{K_{\mathrm{H}}K_{\mathrm{V}}}{\mu K_{\mathrm{SR}}} \tag{24}$$

The fact that these limiting values are not the unity reflects the change of the rotation center of the foundation system with respect to the individual rotation center. Taking this physical interpretation into account, it is possible to establish that the final coupled sway-rocking stiffness correction factor is that of the horizontal stiffness but scaled according to the change of the group rotation center:

$$N = 3: \gamma_{\mathrm{SR}} = \left[1 + \frac{(1-2\nu)}{8\pi}\frac{K_{\mathrm{H}}K_{\mathrm{V}}}{\mu K_{\mathrm{SR}}}\right]\gamma_{\mathrm{H}} \tag{25}$$

$$N = 4: \gamma_{\mathrm{SR}} = \left[1 + \frac{3(1-2\nu)}{16\pi}\frac{K_{\mathrm{H}}K_{\mathrm{V}}}{\mu K_{\mathrm{SR}}}\right]\gamma_{\mathrm{H}} \tag{26}$$

which are shown in Figs. 3 and 4. It is observed that this consideration works very well in practice.

Torsional stiffness By keeping all terms related to the torsion mode of the foundation system: G_{f_1,u_1}, G_{f_1,u_2}, G_{f_1,θ_3}, G_{f_2,u_1}, G_{f_2,u_2}, G_{f_2,θ_3}, G_{m_3,u_1}, G_{m_3,u_2}, G_{m_3,θ_3}; and neglecting the coupled sway-rocking stiffness, the group effect torsional stiffness correction factor can be written as:

$$\gamma_{\mathrm{T}} = \frac{1 + \dfrac{p_2 k_{\mathrm{T}}/k_{\mathrm{H}}}{\tilde{s}^2} + \dfrac{p_3 k_{\mathrm{T}}}{\tilde{s}^3}}{\left(1 + \dfrac{p_2 k_{\mathrm{T}}/k_{\mathrm{H}}}{\tilde{s}^2}\right)\left(1 + \dfrac{q_1 k_{\mathrm{H}}}{\tilde{s}} + \dfrac{q_3 k_{\mathrm{T}}}{\tilde{s}^3} + \dfrac{q_4 k_{\mathrm{H}} k_{\mathrm{T}}}{\tilde{s}^4}\right)} \tag{27}$$

where $k_{\mathrm{T}} = K_{\mathrm{T}}/(\pi\mu D^3)$ is the dimensionless torsional stiffness (isolated foundation), and p and q coefficients are:

$$N = 3: p_2 = 3 \tag{28a}$$

$$p_3 = -(13-9\nu)/4 \tag{28b}$$

$$q_1 = -(2-3\nu)/4 \tag{28c}$$

$$q_3 = -1/4 \tag{28d}$$

$$q_4 = -(1+3\nu)/16 \tag{28e}$$

Note than for the tetrapod ($N = 4$) it has not been possible to obtain a closed-form formula. Figs. 3 and 4 show that the estimation works well for $L/D = 0$, but it quickly degrades as the embedment increases.

3.2 Non-homogeneous soils

In this section, the group effect stiffness correction factors are studied for non-homogeneous soils whose shear modulus follows a power-law with depth ($\mu = \mu_0 \cdot z^\alpha$, $0 \le \alpha \le 1$) and constant Poisson's ratio ν. Fig. 5 shows the correction factors for tetrapod ($N = 4$) and Poisson's ratio $\nu = 0.499$. The left and right columns correspond respectively to $L/D = 1$ and $L/D = 2$, while at each row corresponds to a different stiffness component. For each graph, the corresponding correction factor is calculated for $\alpha = \{0, 0.2, 0.4, 0.6, 0.8, 1\}$.

Results show a great influence of the non-homogeneity exponent α in the vertical and horizontal stiffness correction factors. On the other hand, the influence of the exponent α is particularly small for the rocking and torsional cases, and somewhat more relevant for the coupled sway-rocking stiffness correction factor.

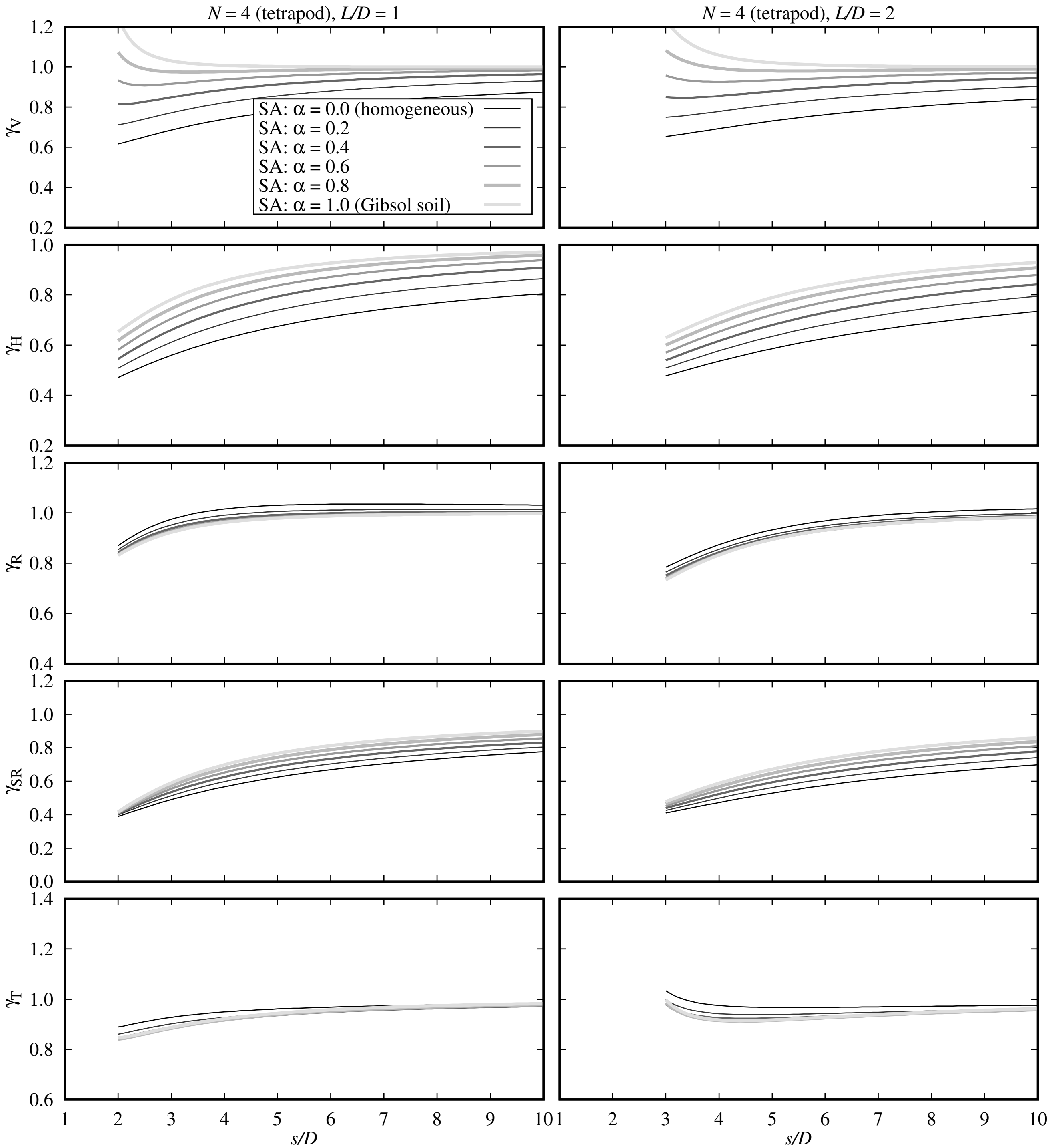

Figure 5: Stiffness correction factors for tetrapod arrangements of rigid suction caisson foundations for non-homogeneous soils ($\nu = 0.499$)

Id	Model	Description
1	Rigid base	Foundation nodes of the superstructure are perfectly fixed.
2	Flexible base without FSFI via master node	Insert the reduced stiffness matrix from Eq. (13) to a master node rigidly linked to the foundation nodes of the superstructure.
3	Flexible base without FSFI	Insert the stiffness matrix $\mathbf{K}_{ii}$ from Eq. (2) to each foundation node of the superstructure.
4	Flexible base with FSFI via master node (closed-form formulas)	Insert the reduced stiffness matrix obtained from Eqs.(17-27,16) to a master node rigidly linked to the foundation nodes of the superstructure.
5	Flexible base with FSFI via master node (numerical)	Insert the reduced stiffness matrix from Eq. (12) to a master node rigidly linked to the foundation nodes of the superstructure.
6	Flexible base with FSFI	Insert the complete stiffness matrix from Eq. (6) to the foundation nodes of the superstructure.
7	Three-dimensional BE-FE model	[Bordón et al., 2017, Bordón et al., 2019]

Table 1: Description of models considered in the usage example

In particular, the increase of the non-homogeneity exponent α reduces the foundation–soil–foundation interaction for the vertical, horizontal and coupled sway-rocking stiffness correction factors, i.e. correction factors approach unity as α increases. This is more severe for the vertical correction factor than for the horizontal or sway-rocking correction factors. In fact, when $\alpha > 0.8$ the vertical stiffness correction factor becomes greater than unity for small spacings.

On the contrary, the increase of the non-homogeneity exponent α increases the foundation–soil–foundation interaction for the rocking and torsional stiffness correction factors, i.e. correction factors move away from unity as α increases. However, the influence of α on these is rather small.

It is possible to find explanation for these phenomena by looking into the Green's function matrix (see Appendix C). It is noticeable that each component contains an inverse distance law of the type $1/r^{b+\alpha} = (1/r^b)\cdot(1/r^\alpha)$, where b is the exponent present in the homogeneous case (see Appendix B). This means that the foundation–soil–foundation interaction reduces faster with the spacing, i.e. there is an additional $1/r^\alpha$ distance scaling factor present in each Green's function component.

4 Usage example

In this section, different ways of using the proposed methodology in a practical problem are described. The problem considers a representative OWT tetrapod jacket with suction caissons taken from [Jalbi and Bhattacharya, 2018]. Fig. 6 shows the geometry of the mentioned tetrapod jacket. The L/D ratio is 1 and the s/D ratio is 3, thus the presented methodology is applicable. The jacket is considered to be made of tubular members of steel ($E_{\text{steel}} = 210$ GPa, $\nu_{\text{steel}} = 0.30$), and rigid joints between members are assumed. A homogeneous soil similar to that used by [Jalbi and Bhattacharya, 2018] is considered: shear modulus $\mu = 3.9$ MPa and Poisson's ratio $\nu = 0.28$. Suction caissons are assumed to be rigid cylindrical foundations, thus formulas from Appendix A can be used.

In order to illustrate the relevance of soil–structure and foundation–soil–foundation interaction in a representative OWT jacket, horizontal and vertical unit displacements are given to the upper four nodes so that horizontal K_x and vertical K_z stiffnesses at the top of the jacket can be measured.

Table 1 and Fig. 7 describe and illustrate the models considered for this usage example, ranging from a simple rigid base model to a rigorous three-dimensional continuum-based flexible base model. The intermediate models increasingly removes the amount of limiting hypothesis such as the foundation-soil-foundation interaction and the master node rigidly connected to foundation nodes. Models from 1 to 6 are built in a in-house standard finite element code, while model 7 is built using a boundary element - finite element code developed by the authors [Bordón et al., 2017, Bordón et al., 2019]. In the latter case, the use of the Mindlin's Green's function reduces the discretisation to only the soil-foundation interface, and thus it incorporates the unbounded domain (half-space) in an exact

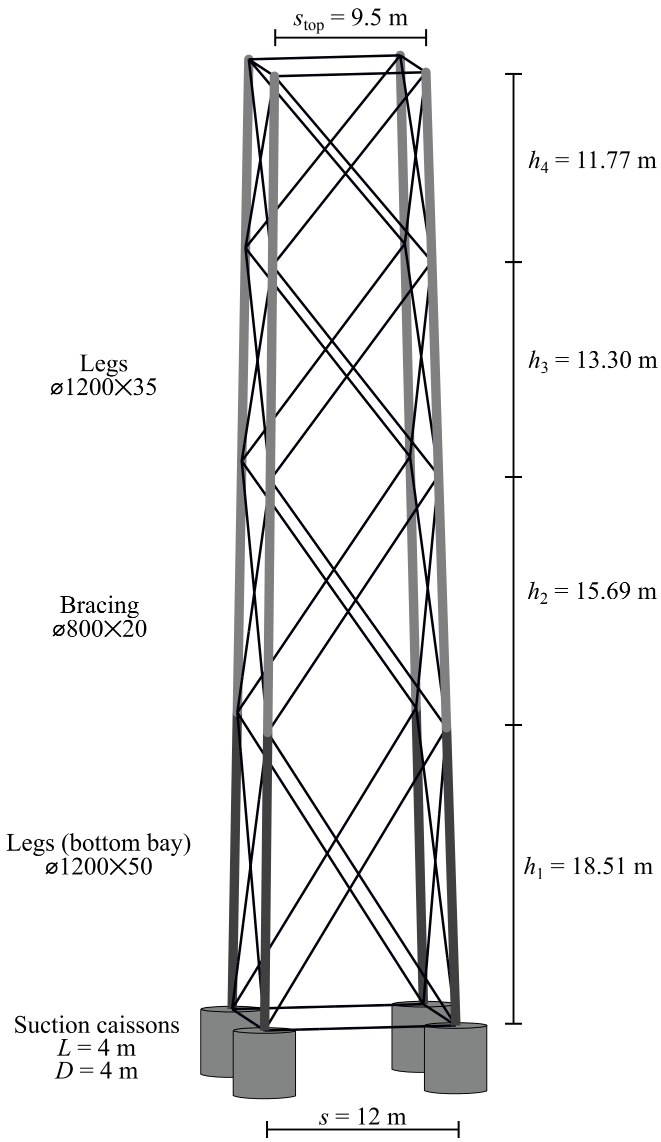

Figure 6: Geometry of the tetrapod jacket with suction caissons

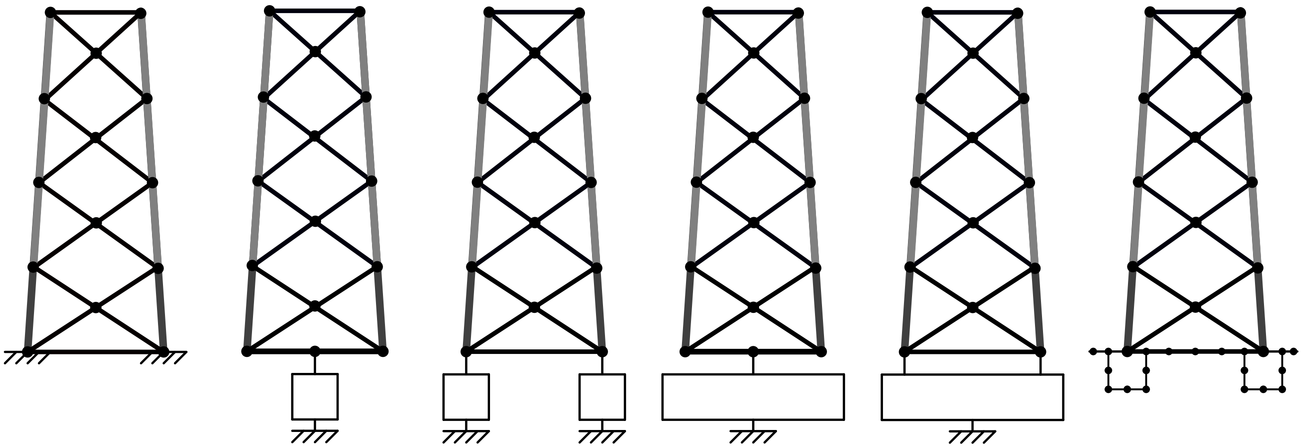

Figure 7: Layout of models considered in the usage example

Model	K_x [MN/m] Value	K_x [MN/m] Dif.*	K_z [MN/m] Value	K_z [MN/m] Dif.*
1	51.255	–	2068.0	–
2	3.7894	-1.4%	285.54	+45.8%
3	3.6012	-6.3%	285.45	+45.7%
4	3.9358	+2.4%	195.71	-0.1%
5	3.9358	+2.4%	195.71	-0.1%
6	3.8189	-0.6%	195.70	-0.1%
7	3.8433	–	195.88	–

*Relative difference between results from models 2-6 with respect to model 7.

Table 2: Summary of results (soil $\mu = 3.9$ MPa)

manner. In all models, jacket tubular members are modelled with two-node Timoshenko finite elements proposed by [Friedman and Kosmatka, 1993].

The resulting stiffnesses at the top of the jacket have been from each one of the seven models, as shown in Table 2. For this example, the relevance of soil–structure interaction is very high since the rigid base model leads to much higher stiffnesses than models with flexible base. For the horizontal stiffness, it is observed a relatively small but relevant influence of foundation–soil–foundation interaction since differences between models 2-3 and models 4-5-6-7 are appreciable. For the vertical stiffness, there is a much higher influence of foundation–soil–foundation interaction since models neglecting it (models 2-3) lead to vertical stiffnesses 46% higher than the reference model (model 7). The hypothesis of considering all foundations rigidly connected (models 2, 4 and 5) have some relevance for the horizontal stiffness, but it becomes unimportant for the vertical stiffness.

For the sake of comparison, a similar study but considering a soil with ten times higher shear modulus ($\mu = 39.0$ MPa) has been performed. Table 3 shows these results. The major difference with the previous results lies in the reduction of the relevance of the soil-structure interaction, since now the differences between the stiffnesses under flexible base and rigid base are smaller. Regarding the performance of each model, the same conclusions as before can be stated.

As seen in Tables 2 and 3 for the horizontal stiffness, model 2 achieves better results than models 3 to 6 despite this model neglects foundation–soil–foundation interaction and also assumes the rigid connection between foundations. By looking into the horizontal stiffness results from the other models, it can be seen that neglecting the foundation–soil–foundation interaction decreases the apparent horizontal stiffness. On the other hand, the assumption of a rigid link between foundations through a master node increases the horizontal stiffness. Therefore, such good result appears to be related to the cancellation of the effects of both hypothesis in this particular case, and hence this model should not

Model	K_x [MN/m]		K_z [MN/m]	
	Value	Dif.*	Value	Dif.*
1	51.255	–	2068.0	–
2	22.753	+2.6%	1273.2	+20.8%
3	20.896	-5.8%	1272.1	+20.8%
4	23.274	+4.9%	1056.9	+0.28%
5	23.274	+4.9%	1056.9	+0.28%
6	22.206	+0.1%	1056.7	+0.27%
7	22.186	–	1053.9	–

*Relative difference between results from models 2-6 with respect to model 7.

Table 3: Summary of results (soil $\mu = 39.0$ MPa)

in general be considered as better to the other richer models.

5 Conclusions

In the present paper, a simple and effective methodology for introducing foundation–soil–foundation interaction in static stiffnesses of multi-element shallow circular foundation systems is presented. In particular, it is applied to tripod and tetrapod arrangements of suction caissons used for Offshore Wind Turbines, including homogeneous and non-homogeneous soils. It is shown that this simple approach works very well for shallow foundations ($L/D \sim 0$), but it also works well for embedded ($L/D \sim 1$) and moderately deep ($L/D \sim 4$) suction caissons as long as the considered dimensionless spacing is $s/D > L/D + 1$. Closed-form expressions for correcting the stiffnesses due to the foundation–soil–foundation interaction are also obtained from the approach.

6 Acknowledgements

The authors are grateful for the support from the Ministerio de Economía y Competitividad (MINECO) of Spain, the Agencia Estatal de Investigación (AEI) of Spain and FEDER through Research Project BIA2017-88770-R.

Notation

α Non-homogeneity exponent for the shear modulus power-law with depth $0 \leq \alpha \leq 1$

γ_{H} Group effect stiffness correction factor for the horizontal stiffness

γ_{R} Group effect stiffness correction factor for the rocking stiffness

γ_{SR} Group effect stiffness correction factor for the coupled sway-rocking stiffness

γ_{T} Group effect stiffness correction factor for the torsional stiffness

γ_{V} Group effect stiffness correction factor for the vertical stiffness

$\mathbf{a}$ Vector of displacements and rotations of a given system of foundations ($6N \times 1$)

$\mathbf{a}_0$ Vector of displacements and rotations of the master node (6×1)

$\mathbf{a}_j$ Vector of displacements and moments of foundation j (6×1)

$\mathbf{D}_j$ Cross-coupled transformation submatrix of a rigid link between foundation j and the master node (3×3)

$\mathbf{G}(\mathbf{x}_j, \mathbf{x}_i)$ Green's function matrix (6×6): displacements and rotations at point $\mathbf{x}_i$ due to forces and moments at point $\mathbf{x}_j$.

$\mathbf{I}_{3\times3}$ 3×3 identity matrix

$\mathbf{K}$ Stiffness matrix for a system of foundations ($6N \times 6N$)

$\mathbf{K}_0$ Stiffness matrix reduced to the master node (6×6)

$\mathbf{K}_0^{\text{int}}$ Stiffness matrix reduced to the master node (6×6) considering foundation–soil–foundation interaction

$\mathbf{K}_0^{\text{no-int}}$ Stiffness matrix reduced to the master node (6×6) without considering foundation–soil–foundation interaction

$\mathbf{p}$ Vector of forces and moments of a given system of foundations ($6N \times 1$)

$\mathbf{p}_0$ Vector of forces and moments reduced to the master node (6×1)

$\mathbf{p}_j$ Vector of forces and moments at foundation j (6×1)

$\mathbf{S}$ Compliance matrix for a system of foundations ($6N \times 6N$)

$\mathbf{S}_{ij}$ Compliance matrix (6×6): displacements and rotations at foundation i due to forces and moments at foudation j.

$\mathbf{T}$ Global transformation matrix of rigid links between a system of foundations and the master node ($6N \times 6$)

$\mathbf{T}_j$ Transformation matrix of a rigid link between foundation j and the master node (6×6)

$\mathbf{x}_0$ Position vector of the master node

$\mathbf{x}_j$ Position vector of foundation j

μ Shear modulus of the soil

μ_0 Shear modulus of the soil at $z = 1$ m (shear modulus power-law with depth)

ν Poisson's ratio of the soil

ν_{steel} Poisson's ratio of steel

$\tilde{s}$ Dimensionless spacing (distance) between closest foundations (polygonal arrangement)

D Foundation diameter

D_j Diameter of foundation j

$d_k^{(j)}$ k component of the relative distance between foundation j and the master node

E_{steel} Young's modulus of steel

G_{f_l,θ_k} Green's function component with gives the rotation in the k direction due to a force in the l direction

G_{f_l,u_k} Green's function component with gives the displacement in the k direction due to a force in the l direction

G_{m_l,θ_k} Green's function component with gives the rotation in the k direction due to a moment in the l direction

G_{m_l,u_k} Green's function component with gives the displacement in the k direction due to a moment in the l direction

K_{H} Horizontal (or lateral) stiffness of an isolated foundation

k_{H} Dimensionless horizontal (or lateral) stiffness of an isolated foundation

$K_{\text{H}}^{\text{int}}$ Horizontal (or lateral) stiffness reduced to the master node considering foundation–soil–foundation interaction

K_{R} Rocking stiffness of an isolated foundation

k_{R} Dimensionless rocking stiffness of an isolated foundation

$K_{\text{R}}^{\text{int}}$ Rocking stiffness reduced to the master node considering foundation–soil–foundation interaction

K_{SR} Coupled sway-rocking stiffness of an isolated foundation

$K_{\text{SR}}^{\text{int}}$ Coupled sway-rocking stiffness reduced to the master node considering foundation–soil–foundation interaction

K_{T} Torsional stiffness of an isolated foundation

k_{T} Dimensionless torsional stiffness of an isolated foundation

$K_{\text{T}}^{\text{int}}$ Torsional stiffness reduced to the master node considering foundation–soil–foundation interaction

K_{V} Vertical stiffness of an isolated foundation

k_{V} Dimensionless vertical stiffness of an isolated foundation

$K_{\text{V}}^{\text{int}}$ Vertical stiffness reduced to the master node considering foundation–soil–foundation interaction

K_x, K_z Horizontal and vertical stiffnesses at the top of the jacket

L	Foundation length
L_j	Embedment length of foundation j
N	Number of foundations
p_k	Numerator coefficient k for closed-form formulas of group effect stiffness correction factors (different for each case)
q_k	Denominator coefficient k for closed-form formulas of group effect stiffness correction factors (different for each case)
r	Distance between foundations and the master node (polygonal arrangement)
s	Spacing (distance) between closest foundations (polygonal arrangement)
t	Foundation/suction caisson skirt thickness
x_k	k cartesian coordinate ($x_1 = x$, $x_2 = y$, $x_3 = z$)
$x_k^{(0)}$	k cartesian coordinate of the master node
$x_k^{(j)}$	k cartesian coordinate of foundation j
${\theta_k}^{(0)}$	k rotation component of the master node
${\theta_k}^{(j)}$	k rotation component at foundation j
${f_k}^{(0)}$	k force component reduced to the master node
${f_k}^{(j)}$	k force component at foundation j
${m_k}^{(0)}$	k moment component reduced to the master node
${m_k}^{(j)}$	k moment component at foundation j
${u_k}^{(0)}$	k displacement component of the master node
${u_k}^{(j)}$	k displacement component at foundation j

7 Appendix A. Stiffnesses of rigid cylindrical foundations in homogeneous half-space

The stiffnesses of a rigid cylindrical foundation of diameter D and depth L ($0 \le L/D \le 6$) perfectly bonded with the surrounding homogeneous soil of shear modulus μ and Poisson' ratio ν ($0 \le \nu < 0.5$) can be approximated by:

$$K_\mathrm{V} = \frac{2\mu D \ln(3-4\nu)}{1-2\nu}\left[1 + 1.08\,(1-0.76\nu)\left(\frac{L}{D}\right)^{0.82}\right] \tag{29a}$$

$$K_\mathrm{H} = \frac{4\mu D}{2-\nu}\left[1 + 1.85\left(\frac{L}{D}\right)^{0.75}\right] \tag{29b}$$

$$K_\mathrm{R} = \frac{\mu D^3}{3\,(1-\nu)}\left[1 + 7.7\,(1-1.2\nu)\left(\frac{L}{D}\right) + 10\,(1-0.7\nu)\left(\frac{L}{D}\right)^{2.5}\right] \tag{29c}$$

$$K_\mathrm{SR} = \frac{11\mu D^2}{4\,(15-17\nu)}\left[1 - 2\nu + 9.7\,(1-1.13\nu)\left(\frac{L}{D}\right) + 11.2\,(1-0.82\nu)\left(\frac{L}{D}\right)^{1.75}\right] \tag{29d}$$

$$K_\mathrm{T} = \frac{2\mu D^3}{3}\left[1 + 5.26\left(\frac{L}{D}\right)^{0.93}\right] \tag{29e}$$

These formulas are enriched versions of those in [Gazetas, 1991] and [Wolf and Deeks, 2004], where each stiffness $K(\mu,\nu,D,L)$ is obtained from the product of the stiffness for the surface footing $K_\mathrm{surface}(\mu,\nu,D)$ and an embedment factor $\kappa(\nu,L/D)$. These were originally developed for embedded foundations, i.e. typically for $L/D \le 1$, but they have been modified in order to be able to reach up to $L/D = 6$ by fitting them to results from a rigorous boundary element model [Bordón et al., 2017]. Fig. 8 shows a comparison between Eqs. (29a-29e) and those of [Wolf and Deeks, 2004] (embedded foundations) and [Poulos and Davis, 1968], [Higgins and Basu, 2011] and [Guo and Randolph, 1996] (pile foundations). As expected, it is observed that they resemble those of [Wolf and Deeks, 2004] for small L/D and they tend to solutions for rigid piles as L/D increases. In this sense, these formulas cover the expected range $0 \le L/D \le 6$ for suction caissons with rigid skirts.

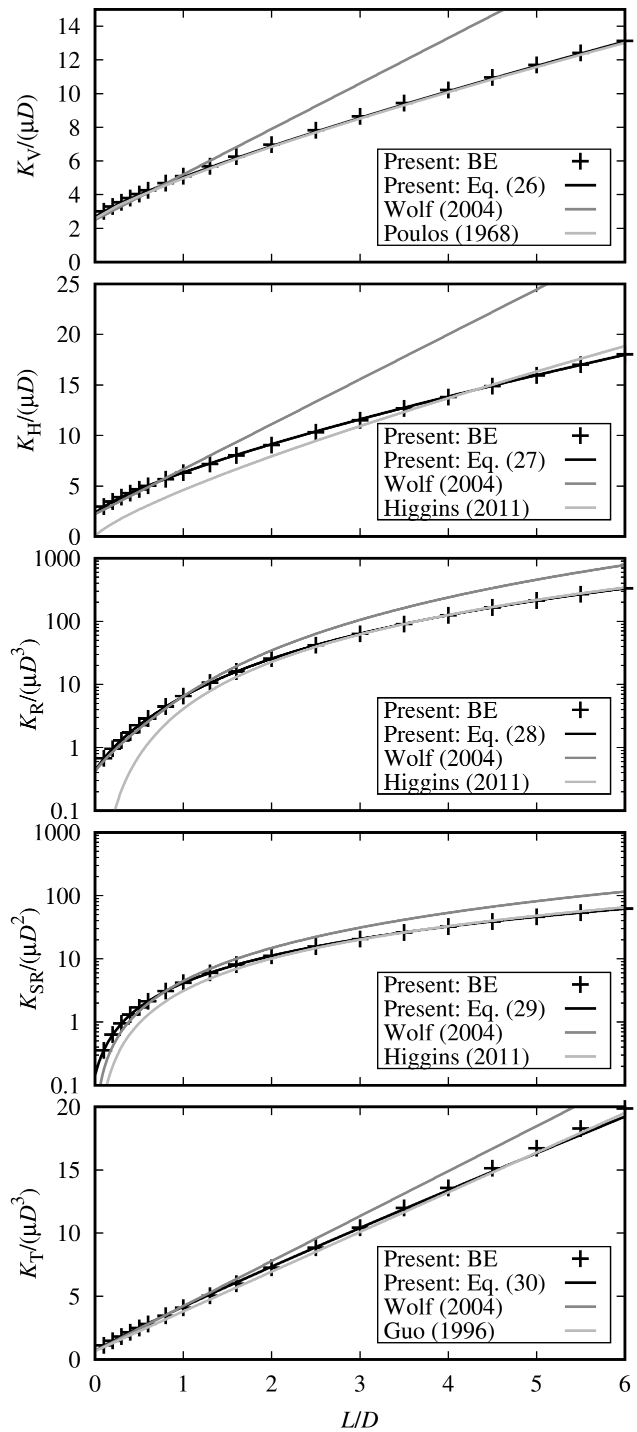

Figure 8: Comparison of Eqs. (29a-29e) against solutions for embedded foundations and pile foundations ($\nu = 0.2$)

8 Appendix B. Complete Green's function for homogeneous half-space

The complete Green's function matrix $\mathbf{G}$ shown in Eq. (4) contains displacements and rotations responses due to point forces and point moments. However, Green's functions are typically presented in the literature only as displacements responses due to point forces, i.e. G_{f_l,u_k}, $l,k = 1,2,3$. Obtaining responses in terms of rotations and loads in terms of point moments is nonetheless a straightforward operation involving derivatives of the usual Green's function in terms of displacements/forces. Starting from G_{f_l,u_k}, i.e. the displacement field at $\mathbf{x}_{\text{obs}}$ due to point forces f_l at $\mathbf{x}_{\text{load}}$, the rest of the Green's function is obtained as follows. The rotation field at $\mathbf{x}_{\text{obs}}$ due a point force f_l at $\mathbf{x}_{\text{load}}$ can be obtained as (see e.g. [Kupradze, 1979, §1.3.2]):

$$G_{f_l,\theta_k} = \frac{1}{2}\left[\nabla \times \left(G_{f_l,u_1}, G_{f_l,u_2}, G_{f_l,u_3}\right)\right] \cdot \mathbf{e}_k \tag{30}$$

where $\nabla = (\partial/\partial x_1^{(\text{obs})}, \partial/\partial x_2^{(\text{obs})}, \partial/\partial x_3^{(\text{obs})})$ and $\mathbf{e}_k$ are the unit vectors in Cartesian coordinates. The displacement field at $\mathbf{x}_{\text{obs}}$ due to a point moment m_l at $\mathbf{x}_{\text{load}}$ can be obtained as (see e.g. "two double forces with moment" from [Love, 1920, Art. 132]):

$$G_{m_l,u_k} = \frac{1}{2}\left[\nabla \times \left(G_{f_1,u_k}, G_{f_2,u_k}, G_{f_3,u_k}\right)\right] \cdot \mathbf{e}_l \tag{31}$$

where $\nabla = (\partial/\partial x_1^{(\text{load})}, \partial/\partial x_2^{(\text{load})}, \partial/\partial x_3^{(\text{load})})$.

For the case of a homogeneous half-space ($x_3 \geq 0$) with shear modulus μ and Poisson's ratio ν, Mindlin's Green's function [Mindlin, 1936] is considered. After performing the above procedure and defining $x_3^{(\text{load})} = x_3^{(\text{obs})} = 0$, $r_k = x_k^{(\text{obs})} - x_k^{(\text{load})}$ for $k = 1,2$, and $r = (r_1^2 + r_2^2)^{1/2}$, the complete 6×6 Green's function matrix can be written as:

$$\mathbf{G}\left(\mathbf{x}_{\text{load}}, \mathbf{x}_{\text{obs}}\right) = \begin{bmatrix} \left[G_{f_l,u_k}\right] & \left[G_{f_l,\theta_k}\right] \\ \left[G_{m_l,u_k}\right] & \left[G_{m_l,\theta_k}\right] \end{bmatrix} \tag{32}$$

where 3×3 sub-matrices are:

$$\left[G_{f_l,u_k}\right] = \begin{bmatrix} \dfrac{r_1^2 + (1-\nu) r_2^2}{2\pi\mu r^3} & \dfrac{\nu r_1 r_2}{2\pi\mu r^3} & \dfrac{(1-2\nu) r_1}{4\pi\mu r^2} \\ G_{f_1,u_2} & \dfrac{(1-\nu) r_1^2 + r_2^2}{2\pi\mu r^3} & \dfrac{(1-2\nu) r_2}{4\pi\mu r^2} \\ -G_{f_1,u_3} & -G_{f_2,u_3} & \dfrac{(1-\nu)}{2\pi\mu r} \end{bmatrix} \tag{33a}$$

$$\left[G_{f_l,\theta_k}\right] = \begin{bmatrix} -\dfrac{(1-2\nu) r_1 r_2}{2\pi\mu r^4} & \dfrac{(1-2\nu)(r_1^2 - r_2^2)}{4\pi\mu r^4} & \dfrac{r_2}{4\pi\mu r^3} \\ G_{f_1,\theta_2} & -G_{f_1,\theta_1} & -\dfrac{r_1}{4\pi\mu r^3} \\ -\dfrac{(1-\nu) r_2}{2\pi\mu r^3} & \dfrac{(1-\nu) r_1}{2\pi\mu r^3} & 0 \end{bmatrix} \tag{33b}$$

$$\left[G_{m_l,u_k}\right] = \begin{bmatrix} G_{f_1,\theta_1} & G_{f_2,\theta_1} & -G_{f_3,\theta_1} \\ G_{f_1,\theta_2} & G_{f_2,\theta_2} & -G_{f_3,\theta_2} \\ -G_{f_1,\theta_3} & -G_{f_2,\theta_3} & 0 \end{bmatrix} \tag{33c}$$

$$\left[G_{m_l,\theta_k}\right] = \begin{bmatrix} \dfrac{(1-\nu)(r_1^2 - 2r_2^2)}{2\pi\mu r^5} & \dfrac{3(1-\nu) r_1 r_2}{2\pi\mu r^5} & 0 \\ G_{m_1,\theta_2} & -\dfrac{(1-\nu)(2r_1^2 - r_2^2)}{2\pi\mu r^5} & 0 \\ 0 & 0 & -\dfrac{1}{8\pi\mu r^3} \end{bmatrix} \tag{33d}$$

The reciprocity principle of the obtained Green's function can be easily verified by observing that $\mathbf{G}\left(\mathbf{x}_{\text{load}}, \mathbf{x}_{\text{obs}}\right) = \left(\mathbf{G}\left(\mathbf{x}_{\text{obs}}, \mathbf{x}_{\text{load}}\right)\right)^T$.

9 Appendix C. Complete Green's function for non-homogeneous half-space

Following the same steps and notation as in Appendix B, the complete Green's function matrix $\mathbf{G}$ shown in Eq. (4) is here presented for the case of a non-homogeneous half-space whose shear modulus follows a power-law with depth

($\mu = \mu_0 \cdot z^\alpha$, $0 \leq \alpha \leq 1$) and constant Poisson's ratio ν. For source and observation points at the free-surface ($x_3^{(\text{load})} = x_3^{\text{obs}} = 0$), the corresponding Green's function matrix is in closed-form, see Booker et al. [Booker et al., 1985]. By defining the following constants:

$$\beta = \sqrt{(1+\alpha)\left(1 - \frac{\alpha\nu}{1-\nu}\right)} \tag{34a}$$

$$\Omega_\alpha = \frac{\Gamma\left(\frac{1+\alpha}{2}\right) \cdot \Gamma\left(\frac{1}{2}\right)}{\Gamma\left(\frac{2+\alpha}{2}\right)} \tag{34b}$$

$$F_{\alpha\beta} = \frac{2^{\alpha+1}(\alpha+2)}{\pi} \frac{\Gamma\left(\frac{3+\alpha+\beta}{2}\right)\Gamma\left(\frac{3+\alpha-\beta}{2}\right)}{\Gamma(3+\alpha)} \tag{34c}$$

$$b = \frac{(1-\nu^2)\beta \sin(\beta\pi/2)}{\alpha(1+\alpha)} F_{\alpha\beta} \tag{34d}$$

$$k = \frac{2(1+\nu)}{\alpha\Omega_\alpha} \tag{34e}$$

$$h = \frac{\left(1-\nu^2\right)(1+\alpha)\sin(\beta\pi/2)}{\alpha\beta} F_{\alpha\beta} \tag{34f}$$

$$l = -\frac{(1-\nu^2)\cos(\beta\pi/2)}{\alpha} F_{\alpha\beta} \tag{34g}$$

$$L = l/\Omega_\alpha \tag{34h}$$

$$B = b/\Omega_{\alpha-1} \tag{34i}$$

$$K = \frac{1}{2}\left[\frac{h+k}{\Omega_{\alpha-1}} - \frac{h-k}{2\Omega_{\alpha+1} - \Omega_{\alpha-1}}\right] \tag{34j}$$

$$H = \frac{1}{2}\left[\frac{h+k}{\Omega_{\alpha-1}} + \frac{h-k}{2\Omega_{\alpha+1} - \Omega_{\alpha-1}}\right] \tag{34k}$$

the complete 6×6 Green's function matrix can be written as:

$$[G_{f_l,u_k}] = \begin{bmatrix} \frac{Hr_1^2 + Kr_2^2}{E_0 r^{3+\alpha}} & \frac{(H-K)\, r_1 r_2}{E_0 r^{3+\alpha}} & \frac{Lr_1}{E_0 r^{2+\alpha}} \\ G_{f_1,u_2} & \frac{Kr_1^2 + Hr_2^2}{E_0 r^{3+\alpha}} & \frac{Lr_2}{E_0 r^{2+\alpha}} \\ -G_{f_1,u_3} & -G_{f_2,u_3} & \frac{B}{E_0 r^{1+\alpha}} \end{bmatrix} \tag{35a}$$

$$[G_{f_l,\theta_k}] = \begin{bmatrix} -\frac{Lr_1 r_2 (2+\alpha)}{E_0 r^{4+\alpha}} & \frac{L\left[(1+\alpha) r_1^2 - r_2^2\right]}{E_0 r^{4+\alpha}} & \frac{r_2 (H + K\alpha)}{2E_0 r^{3+\alpha}} \\ \frac{L\left[r_1^2 - (1+\alpha)\, r_2^2\right]}{E_0 r^{4+\alpha}} & -G_{f_1,\theta_1} & -\frac{r_1 (H+K\alpha)}{2E_0 r^{3+\alpha}} \\ -\frac{Br_2 (1+\alpha)}{E_0 r^{3+\alpha}} & \frac{Br_1 (1+\alpha)}{E_0 r^{3+\alpha}} & 0 \end{bmatrix} \tag{35b}$$

$$[G_{m_l,u_k}] = \begin{bmatrix} G_{f_1,\theta_1} & G_{f_2,\theta_1} & -G_{f_3,\theta_1} \\ G_{f_1,\theta_2} & G_{f_2,\theta_2} & -G_{f_3,\theta_2} \\ -G_{f_1,\theta_3} & -G_{f_2,\theta_3} & 0 \end{bmatrix} \tag{35c}$$

$$\frac{[G_{m_l,\theta_k}]}{1+\alpha} = \begin{bmatrix} \frac{B\left[r_1^2 - (2+\alpha)\, r_2^2\right]}{E_0 r^{5+\alpha}} & \frac{Br_1 r_2 (3+\alpha)}{E_0 r^{5+\alpha}} & 0 \\ \frac{Br_1 r_2 (3+\alpha)}{E_0 r^{5+\alpha}} & -\frac{B\left[(2+\alpha)\, r_1^2 - r_2^2\right]}{E_0 r^{5+\alpha}} & 0 \\ 0 & 0 & -\frac{H+K\alpha}{4E_0 r^{3+\alpha}} \end{bmatrix} \tag{35d}$$

where $E_0 = 2\mu_0(1+\nu)$, $r_k = x_k^{(\text{obs})} - x_k^{(\text{load})}$ for $k = 1, 2$, and $r = (r_1^2 + r_2^2)^{1/2}$. In Eqs. (34b-34c), $\Gamma(x)$ is the Gamma function.

References

[Booker et al., 1985] Booker, J. R., Balaam, N. P., and Davis, E. H. (1985). The behaviour of an elastic non-homogeneous half-space. Part I – line and point loads. *International Journal for Numerical and Analytical Methods in Geomechanics*, 9:353–367.

[Bordón et al., 2017] Bordón, J. D. R., Aznárez, J. J., and Maeso, O. (2017). Dynamic model of open shell structures buried in poroelastic soils. *Computational Mechanics*, 60(2):269–288.

[Bordón et al., 2019] Bordón, J. D. R., Aznárez, J. J., Padrón, L. A., Maeso, O., and Bhattacharya, S. (2019). Closed-form stiffnesses of multi-bucket foundations for OWT including group effect correction factors. *Marine Structures*, 65:326–342.

[Cook et al., 1989] Cook, R. D., Malkus, D. S., and Plesha, M. E. (1989). *Concepts and applications of finite element analysis*. John Wiley & Sons, third edition.

[Doherty and Deeks, 2003] Doherty, J. P. and Deeks, A. J. (2003). Elastic response of circular footings embedded in a non-homogeneous half-space. *Géotechnique*, 53(8):703–714.

[Doherty et al., 2005] Doherty, J. P., Houlsby, G. T., and Deeks, A. J. (2005). Stiffness of flexible caisson foundations embedded in nonhomogeneous elastic soil. *Journal of Geotechnical and Geoenvironmental Engineering*, 131(12):1498–1508.

[Domínguez, 1993] Domínguez, J. (1993). *Boundary Elements in Dynamics*. International Series on Computational Engineering. Computational Mechanics Publications.

[Efthymiou and Gazetas, 2018] Efthymiou, G. and Gazetas, G. (2018). Elastic stiffnesses of a rigid suction caisson and its cylindrical sidewall shell. *Journal of Geotechnical and Geoenvironmental Engineering*, 145(2):06018014.

[Friedman and Kosmatka, 1993] Friedman, Z. and Kosmatka, J. (1993). An improved two-node timoshenko beam finite element. *Computers & Structures*, 47(3):473 – 481.

[Gazetas, 1991] Gazetas, G. (1991). Formulas and charts for impedances of surface and embedded foundations. *Journal of Geotechnical Engineering*, 117(9):1363–1381.

[Guo and Randolph, 1996] Guo, W. D. and Randolph, M. F. (1996). Torsional piles in non-homogeneous media. *Computers and Geotechnics*, 19(4):265–287.

[Higgins and Basu, 2011] Higgins, W. and Basu, D. (2011). Fourier finite element analysis of laterally loaded piles in elastic media. Internal Geotechnical Report 2011-1, Department of Civil and Environmental Engineering, University of Connecticut.

[Houlsby and Byrne, 2005a] Houlsby, G. T. and Byrne, B. W. (2005a). Design procedures for installation of suction caissons in clay and other materials. *Proceedings of the Institution of Civil Engineers*, 158(GE2):75–82.

[Houlsby and Byrne, 2005b] Houlsby, G. T. and Byrne, B. W. (2005b). Design procedures for installation of suction caissons in sand. *Proceedings of the Institution of Civil Engineers*, 158(GE3):135–144.

[Jalbi and Bhattacharya, 2018] Jalbi, S. and Bhattacharya, S. (2018). Closed form solution for the first natural frequency of offshore wind turbine jackets supported on multiple foundations incorporating soil-structure interaction. *Soil Dynamics and Earthquake Engineering*, 113:593–613.

[Kupradze, 1979] Kupradze, V. D., editor (1979). *Three-dimensional problems of the mathematical theory of elasticity and thermoelasticity*, volume 25 of *Applied Mathematics and Mechanics*. North-Holland, first edition.

[Love, 1920] Love, A. E. H. (1920). *A treatise on the mathematical theory of elasticity*. Cambridge University Press, third edition.

[Mindlin, 1936] Mindlin, R. D. (1936). Force at a point in the interior of a semi-infinite solid. *Journal of Applied Physics*, 7:195–202.

[Poulos and Davis, 1968] Poulos, H. G. and Davis, E. H. (1968). The settlement behaviour of single axially loaded incompressible piles and piers. *Géotechnique*, 18:351–371.

[Poulos and Davis, 1974] Poulos, H. G. and Davis, E. H. (1974). *Elastic solution for soil and rock mechanics*. John Wiley & Sons, New York.

[Poulos and Davis, 1980] Poulos, H. G. and Davis, E. H. (1980). *Pile foundation analysis and design*. Rainbow-Bridge Book Co.

[Randolph and Wroth, 1979] Randolph, M. F. and Wroth, C. P. (1979). An analysis of the vertical deformation of pile groups. *Géotechnique*, 29(4):423–439.

[Wolf, 1985] Wolf, J. P. (1985). *Dynamic soil-structure interaction*. Civil Engineering and Engineering Mechanics. Prentice-Hall, Inc.

[Wolf and Deeks, 2004] Wolf, J. P. and Deeks, A. J. (2004). *Foundation Vibration Analysis: A Strength-of-Materials Approach*. Elsevier.

[Wong, 1975] Wong, H. L. (1975). *Dynamic soil-structure interaction*. PhD thesis, California Institute of Technology.

[Wong and Luco, 1986] Wong, H. L. and Luco, J. E. (1986). Dynamic interaction between rigid foundations in a layered half-space. *Soil Dynamics and Earthquake Engineering*, 5(3):149–158.